Extracellular superoxide dismutase is important for hippocampal neurogenesis and preservation of cognitive functions after irradiation

Yani Zou[a], Rikki Corniola[a], David Leu[a,b], Aslam Khan[a,b], Peyman Sahbaie[c,d], Ayanabha Chakraborti[e], David J. Clark[c,d], John R. Fike[e,f], and Ting-Ting Huang[a,b,1]

[a]Department of Neurology and Neurological Sciences and [d]Department of Anesthesia, Stanford University, Stanford, CA 94304; [b]Geriatric Research, Education and Clinical Center, and [c]Anesthesiology Service, Veteran's Affairs Palo Alto Health Care System, Palo Alto, CA 94304; and [e]Department of Neurological Surgery and [f]Department of Radiation Oncology, University of California, San Francisco, CA 94143

Edited by James E. Cleaver, University of California, San Francisco, CA, and approved November 19, 2012 (received for review September 27, 2012)

Cranial irradiation is widely used in cancer therapy, but it often causes cognitive defects in cancer survivors. Oxidative stress is considered a major cause of tissue injury from irradiation. However, in an earlier study mice deficient in the antioxidant enzyme extracellular superoxide dismutase (EC-SOD KO) showed reduced sensitivity to radiation-induced defects in hippocampal functions. To further dissect the role of EC-SOD in neurogenesis and in response to irradiation, we generated a bigenic EC-SOD mouse model (OE mice) that expressed high levels of EC-SOD in mature neurons in an otherwise EC-SOD–deficient environment. EC-SOD deficiency was associated with reduced progenitor cell proliferation in the subgranular zone of dentate gyrus in KO and OE mice. However, high levels of EC-SOD in the granule cell layer supported normal maturation of newborn neurons in OE mice. Following irradiation, wild-type mice showed reduced hippocampal neurogenesis, reduced dendritic spine densities, and defects in cognitive functions. OE and KO mice, on the other hand, were largely unaffected, and the mice performed normally in neurocognitive tests. Although the resulting hippocampal-related functions were similar in OE and KO mice following cranial irradiation, molecular analyses suggested that they may be governed by different mechanisms: whereas neurotrophic factors may influence radiation responses in OE mice, dendritic maintenance may be important in the KO environment. Taken together, our data suggest that EC-SOD plays an important role in all stages of hippocampal neurogenesis and its associated cognitive functions, and that high-level EC-SOD may provide protection against irradiation-related defects in hippocampal functions.

Cranial irradiation is widely used as a treatment modality for patients with primary or metastatic brain tumors (1–3), and is also used as a prophylactic treatment to prevent metastases of high-risk tumors to the nervous system (4). Although effective, cranial irradiation is associated with various complications or side effects in cancer survivors (1–3). One of the severe complications is neurocognitive impairment, which can include defects in executive functions and learning and memory (3). Neurocognitive impairments occur in both adults and children and are generally associated with higher doses and younger age (3). The pathogenesis of radiation-induced neurocognitive impairment is not completely understood, but recent studies suggest that suppressed hippocampal neurogenesis (5, 6), increased hippocampal neuronal apoptosis (7, 8), and reduced growth hormone secretion (9, 10) may be involved.

The production of reactive oxygen species (ROS) is considered a major cause of radiation-induced tissue damage (11). Ionizing irradiation not only results in the acute generation of short-lived ROS, it also results in a persistent state of oxidative stress that extends up to several months or even years after irradiation (12, 13). Accordingly, animal and cell models with altered antioxidant capacities have been used to investigate the biochemical pathways involved in radiation-induced tissue and cell injuries, and experimental antioxidant-based therapies have been designed to protect normal tissues during radiation treatments (14).

Hippocampal neurogenesis is important for hippocampal-dependent functions of learning and memory and the process is exquisitely sensitive to suppression by various stressors, including radiation and oxidative stress (5, 6, 15). To determine if altered redox balance in the hippocampal microenvironment affects hippocampal neurogenesis and the associated functions of learning and memory, we used a knockout mouse model (KO) deficient in the extracellular antioxidant enzyme, EC-superoxide dismutase (EC-SOD), in an earlier study with cranial irradiation (13, 16). When examined at 3–4 mo of age, EC-SOD deficiency was associated with a significant suppression of baseline neurogenesis and impaired hippocampal-dependent cognitive functions (13, 16). Unexpectedly, EC-SOD deficiency also rendered the process less sensitive to radiation-induced changes. The underlining mechanism for this paradoxical finding was not clear, but preliminary studies ruled out up-regulation of major antioxidant enzymes (13). The results suggested that the interaction between redox balance and irradiation and their effects on hippocampal functions can be complex, and understanding how these elements work in concert may be a key to identifying strategies for radioprotection.

To manipulate redox balance in the hippocampus, we generated a mouse model with inducible EC-SOD transgenes (17). In the current study, we combined the inducible transgenes with EC-SOD KO and generated a bigenic mouse model, designated as the overexpressor (OE), with high levels of EC-SOD expressed only in Ca/calmodulin-dependent protein kinase- (CaMKII) positive neurons in an otherwise EC-SOD–deficient environment (17). Hippocampal neurogenesis generates new granule cells that are functionally integrated into the hippocampal network (18). Because granule cells are CaMKII-positive neurons and are the principal excitatory neurons in the dentate gyrus, the manipulation leads to an estimated four- to fivefold increase in EC-SOD activity in the hippocampal formation in OE mice (17). The OE mice were used to investigate the effects of altered EC-SOD levels at different stages of hippocampal neurogenesis and the functional consequences of learning and memory. Comparison between WT, OE, and KO mice revealed the importance of EC-SOD in progenitor cell proliferation, dendritic development, and long-term survival of newborn neurons. The study results also suggested that

Author contributions: Y.Z., R.C., J.R.F., and T.-T.H. designed research; Y.Z., R.C., D.L., A.K., P.S., and A.C. performed research; D.J.C. contributed new reagents/analytic tools; Y.Z., R.C., P.S., A.C., and T.-T.H. analyzed data; and Y.Z., J.R.F., and T.-T.H. wrote the paper.

The authors declare no conflict of interest.

This article is a PNAS Direct Submission.

[1]To whom correspondence should be addressed. E-mail: tthuang@stanford.edu.

This article contains supporting information online at www.pnas.org/lookup/suppl/doi:10.1073/pnas.1216913110/-/DCSupplemental.

maintenance of the dendritic system following cranial irradiation was important for preservation of neurocognitive functions.

Results

EC-SOD Level Affects Neurocognitive Functions. To determine if altered EC-SOD levels influenced neurocognitive functions, we carried out radial-arm water maze (RAWM) and novel location recognition (NLR) tests 1 mo after a single dose (5 Gy) of cranial irradiation (Fig. 1*A*). In these two studies, animals with normal spatial memory would make fewer mistakes by the end of the RAWM test and recognize objects in a novel location by increasing investigation time in the NLR test.

RAWM results showed that sham-irradiated WT and OE mice significantly reduced incorrect arm entries (i.e., errors, 36% and 48% reduction, respectively) at the end of the test, whereas sham-irradiated KO were not able to make significant improvement (Fig. 1*B*). Following irradiation, WT mice lost the ability to reduce errors, but OE mice maintained (two-way ANOVA, Bonferroni posttest, $t = 2.89$, $P < 0.05$) and KO mice improved ($t = 3.56$, $P < 0.01$) their ability to significantly reduce errors made at the end of the test (Fig. 1*B*). Despite differences in the number of errors made before reaching the platform, all mice significantly reduced the time spent reaching the target platform (Fig. 1*C*). There was also no significant difference in the number of errors made or time required to reach the platform among animals within the same treatment group.

In NLR tests, sham-irradiated WT ($t = 3.71$, $P < 0.01$) and KO ($t = 4.76$, $P < 0.001$) mice recognized the novel placement of the object and spent significantly more time investigating the object in its new location, but sham-irradiated OE mice were indifferent to the new location (Fig. 1*D* and Fig. S1). Following irradiation, WT mice failed to recognize the novel location, but OE ($t = 5.64$, $P < 0.001$) and KO ($t = 4.92$, $P < 0.001$) mice all spent significantly more time investigating the object in its new location (Fig. 1*D*). Taken together, these data suggested that both sham-irradiated OE and KO mice had some learning defects; however, following irradiation, these particular defects in hippocampal-dependent learning were largely corrected. Similar to RAWM findings, no significant difference in the exploration ratio for the novel location was observed across different cohorts.

Whereas NLR relies on hippocampal functions, novel object recognition (NOR) is independent of hippocampus (19). Despite differences in NLR results, both sham and irradiated WT and OE mice had no trouble recognizing a new object in the NOR test and spent significantly more time investigating the new object (Fig. 1*E* and Fig. S1). On the other hand, sham and irradiated KO mice were not able to significantly discern the difference between a novel and a familiar object (Fig. 1*E* and Fig. S1).

Additionally, open field and elevated zero maze tests were carried out to determine motor activities and anxiety levels. Although sham-irradiated OE mice spent significantly less amount of time in the center 50% area of an open field, no significant differences were observed in the elevated zero maze paradigm (Fig. S2).

In the behavioral field, contextual fear conditioning is commonly used to test hippocampal-dependent learning. However, preliminary studies with OE and KO mice showed both to be more sensitive to tactile and heat stimulation (Fig. S3). Although there was no direct correlation, increased tactile and heat sensitivity suggested that OE and KO mice might be more sensitive to electrical stimulation in the contextual fear-conditioning paradigm, which might result in enhanced freezing response and affect the data interpretation. Consequently, a contextual fear-conditioning test was not performed with these mice.

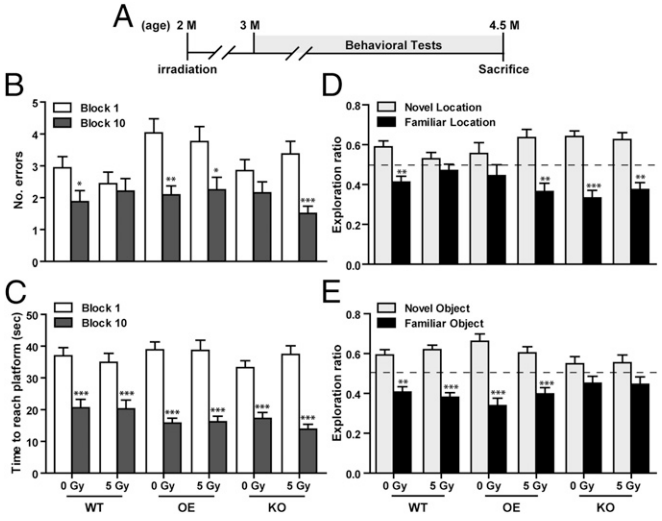

Fig. 1. Effects of EC-SOD and irradiation on hippocampal-dependent learning and memory. (*A*) Experimental timeline. Sham and irradiated (5 Gy) mice were subjected to various behavioral tests starting at 3 mo of age, and all tests were concluded by 4.5 mo of age. (*B* and *C*) Radial-arm water maze. Comparison of errors made in arm entry (*B*) [$F_{(1,168)} = 32.11$, $P < 0.0001$] and time spent to reach the platform (*C*) [$F_{(1,214)} = 198$, $P < 0.0001$)] in the beginning (block 1) and the end (block 10) of the test. (*D* and *E*) NLR and NOR tests. Comparison of exploration ratio for investigation of an object in a novel vs. familiar location (*D*) [$F_{(1,174)} = 78.50$, $P < 0.0001$)] or a novel vs. a familiar object (*E*) [$F_{(1,172)} = 105.9$, $P < 0.0001$]. The dashed line in *D* and *E* represents exploration by chance (i.e., exploration ratio of 0.5) between novel and familiar location or object. Data are presented as mean ± SEM. Two-way ANOVA with Bonferroni posttest was carried out. $*P < 0.05$, $**P < 0.01$, $***P < 0.001$ for postanalysis comparing between block 1 and block 10 or between novel and familiar location or object within each genotype and treatment. $n = 17$–20 mice per genotype per treatment.

EC-SOD Affects Progenitor Cell Proliferation and Long-Term Survival. To determine if differences in neurocognitive functions were associated with changes in hippocampal neurogenesis, a 7-d BrdU injection protocol was carried out and the production and maturation of newborn cells in the subgranular zone (SGZ) of the dentate gyrus was assessed 4 wk after the first BrdU injection (Fig. 2*A*). Compared with sham-irradiated WT controls, there was an 81% reduction ($t = 11.45$, $P < 0.001$) in the total number of newly generated cells ($BrdU^+$) in sham-irradiated KO mice (Fig. 2*B*). Reconstitution of high levels of EC-SOD in granule cells, on the other hand, substantially increased total number of $BrdU^+$ cells in OE mice (OE vs. KO, $t = 7.85$, $P < 0.001$), although the level was still 27% lower than that in WT mice ($t = 4.21$, $P < 0.001$) (Fig. 2*B*). Irradiation led to a significant reduction in total $BrdU^+$ cells in WT mice (51% reduction, $t = 4.45$, $P < 0.001$), but no significant changes were observed in irradiated OE or KO mice (Fig. 2*B*). Consequently, total $BrdU^+$ cells in irradiated OE was 1.7-fold and 2.3-fold higher than that of irradiated WT and KO, respectively (Fig. 2*B* and Table S1).

To determine the lineage preference of newborn $BrdU^+$ cells, their identities as mature neurons ($NeuN^+$) or astroglia ($GFAP^+$) were examined. No significant difference in the percentage of $BrdU^+$ cells that matured into neurons ($BrdU^+/NeuN^+$) or astroglia ($BrdU^+/GFAP^+$) was observed among the sham-irradiated groups (Fig. 2 *C* and *D*), suggesting that differences in EC-SOD levels did not affect lineage determination. Following irradiation, the percentage of $BrdU^+/NeuN^+$ cells declined significantly but the percentage of $BrdU^+/GFAP^+$ cells increased significantly in WT and KO mice (Fig. 2 *C* and *D* and Table S1). However, no significant changes were observed in irradiated OE mice (Fig. 2 *C* and *D*). After converting the percentage to total number of newborn neurons and glia, the profile of $BrdU^+/NeuN^+$ cell numbers (Fig. 2*E*) was similar to that of $BrdU^+$ cells (Fig. 2*B*). On the other hand, the number of newborn astroglia in sham-irradiated WT was significantly higher than that in sham-irradiated OE and KO mice, but

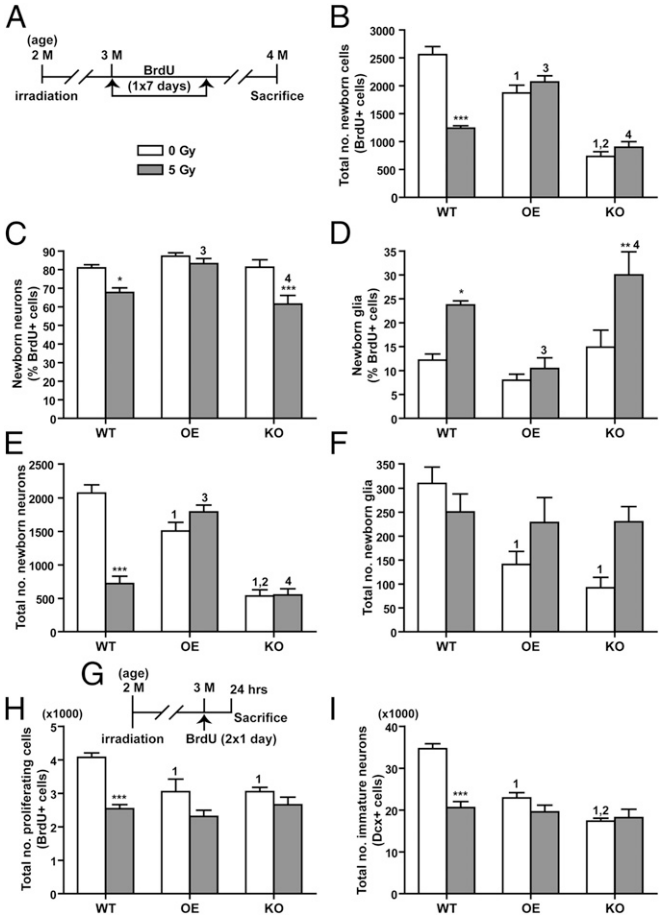

Fig. 2. Hippocampal neurogenesis following cranial irradiation. (*A*) Experimental timeline for identifying long-term survival of newly born cells. (*B*) Total number of mature BrdU$^+$ cells in the SGZ of hippocampal dentate gyrus. There was a significant interaction between genotype and treatment [$F_{(2,32)} = 26.39$, $P < 0.0001$]. Both irradiation [$F_{(1,32)} = 11.95$, $P = 0.0016$] and genotype [$F_{(2,32)} = 70.74$, $P < 0.0001$] played a significant role in the data variation. (*C*) Newly born neurons as percentage of BrdU$^+$ cells in the SGZ. There was a significant interaction between genotype and treatment. Both irradiation [$F_{(1,33)} = 18.85$, $P = 0.0001$] and genotype [$F_{(2,33)} = 8.82$, $P = 0.0009$] played a significant role in the data variation. (*D*) Newly generated glia as percentage of BrdU$^+$ cells in the SGZ. There was a significant interaction between genotype and treatment. Both irradiation [$F_{(1,33)} = 14.63$, $P = 0.0006$] and genotype [$F_{(2,33)} = 9.38$, $P = 0.0006$] played a significant role in the data variation. (*E*) Total number of newborn neurons (BrdU$^+$/NeuN$^+$ double-positive cells) in the SGZ. (*F*) Total number of newborn glia (BrdU$^+$/GFAP$^+$ cells) in the SGZ. (*G*) Experimental timeline for identifying proliferating cells with BrdU labeling. (*H*) Total number of BrdU$^+$ cells, captured within a 24-h window, as a function of progenitor cell proliferation. There was a significant interaction between genotype and treatment [$F_{(2,26)} = 3.75$, $P = 0.037$]. Both irradiation [$F_{(1,26)} = 26.45$, $P < 0.0001$] and genotype [$F_{(2,26)} = 4.27$, $P = 0.0248$] played a significant role in the data variation. (*I*) Total number of immature neurons (Dcx$^+$ cells) in the SGZ at 1 mo following cranial irradiation. There was a significant interaction between genotype and treatment [$F_{(2,24)} = 26.58$, $P < 0.0001$]. Genotype also played a significant role in the data variation [$F_{(2,24)} = 22.19$, $P < 0.0001$]. Data are presented as mean ± SEM. Two-way ANOVA with Bonferroni posttest was carried out. *$P < 0.05$, ***$P < 0.001$ for comparison between 0 and 5 Gy within each genotype. 1, $P < 0.05$ compared with WT/0 Gy; 2, $P < 0.05$ compared with OE/0 Gy; 3, $P < 0.05$ compared with WT/5 Gy; 4, $P < 0.05$ compared with OE/5 Gy. $n = 5$–8 mice per genotype per treatment.

no significant difference in the number of BrdU$^+$/GFAP$^+$ cells was observed among the irradiated groups (Fig. 2*F*).

Depending on the activation state, activated microglia can be detrimental or beneficial to neurogenesis in adult brains (20–22). To know if the activated microglia population was altered by EC-SOD levels or irradiation, total number of CD68$^+$ cells in the dorsal hippocampal area was determined. The number of CD68$^+$ cells was comparable among all sham-irradiated groups and significant increases were observed in all three groups following irradiation, with OE mice showing the largest increase. Consequently, the number of CD68$^+$ cells in irradiated OE mice was significantly higher than that in irradiated WT and KO mice (Fig. S4).

To determine if increased production and maturation of new neurons was because of increased progenitor cell proliferation or commitment to the neuronal lineage, a short-term BrdU labeling (Fig. 2*G*) was carried out to identify proliferating cells. The number of immature neurons (doublecortin; Dcx$^+$ cells) was also determined. In sham-irradiated mice, the total number of BrdU$^+$ cells counted in the SGZ of OE ($t = 3.39$, $P < 0.01$) and KO ($t = 3.76$, $P < 0.01$) mice was 75% that of WT mice (Fig. 2*H*); the total Dcx$^+$ cells in OE ($t = 5.86$, $P < 0.001$) and KO ($t = 8.63$, $P < 0.001$) mice were 66% and 50% that of WT controls (Fig. 2*I*), respectively. Following irradiation, total numbers of BrdU$^+$ and Dcx$^+$ cells in WT mice were reduced by 38% ($t = 4.79$, $P < 0.001$) and 41% ($t = 7.02$, $P < 0.001$), respectively. OE and KO mice, on the other hand, did not show significant reductions in total BrdU$^+$ or Dcx$^+$ cells from irradiation (Fig. 2 *H* and *I*). Consequently, no significant difference in total number of BrdU$^+$ or Dcx$^+$ cells was observed among irradiated WT, OE, and KO mice. Taken together, the results suggested that EC-SOD deficiency decreased progenitor cell proliferation and long-term survival of newborn cells in the SGZ, that reconstitution of high levels of EC-SOD in granule cells significantly enhanced long-term survival of newborn cells, and that EC-SOD OE and KO mice were not susceptible to radiation-induced suppression of neurogenesis.

EC-SOD and Irradiation Affect the Dendritic System. We noticed that Dcx$^+$ cells from OE mice had a more elaborate pattern of dendritic arborization (Fig. 3*A*), suggesting that Dcx$^+$ cells in OE mice may be more mature. Examination of Dcx$^+$ cells with secondary dendritic branching (i.e., categories E and F cells) (23) showed the number of mature Dcx$^+$ cells to be significantly higher in sham-irradiated OE (OE vs. WT, $t = 3.89$, $P < 0.01$) and significantly lower in sham-irradiated KO mice (KO vs. WT, $t = 3.23$, $P < 0.01$) (Fig. 3*B*), suggesting a positive association between the number of mature Dcx$^+$ cells and EC-SOD levels. Irradiation did not lead to a significant change in the number of categories E and F Dcx$^+$ cells in all three genotypes.

To determine if differences in dendritic arborization persisted as newborn neurons matured, intracranial injection of retrovirus was carried out to label new neurons with GFP. Morphological analysis was carried out 4 wk later to allow time for maturation. Study results showed that GFP$^+$/NeuN$^+$ cells in WT mice were well integrated into the granule cell layer, with secondary and tertiary dendrites branching into the molecular layer (Fig. 3*C*). In comparison, GFP$^+$/NeuN$^+$ cells in OE mice started branching earlier and some cells even had multiple primary dendrites. These newborn neurons also showed more complex dendritic arborization (Fig. 3*D*), but the dendrites did not reach as far into the molecular layer as WT mice. Consequently, total dendritic lengths and number of branches were not significantly different between WT and OE (Fig. S5). KO mice, on the other hand, had minimal dendritic arborization (Fig. 3*D*), which resulted in significantly fewer dendritic branches and shorter dendritic lengths (Fig. S5).

To further ascertain the effects of EC-SOD and irradiation on the dendritic system, spine densities were analyzed. No significant differences were observed among the sham-irradiated groups (Fig. 3*E*). Following irradiation, significant decreases in spine densities were observed in WT mice ($t = 3.05$, $P < 0.05$); however, no significant changes were observed in OE and KO mice (Fig. 3*E* and Table S1).

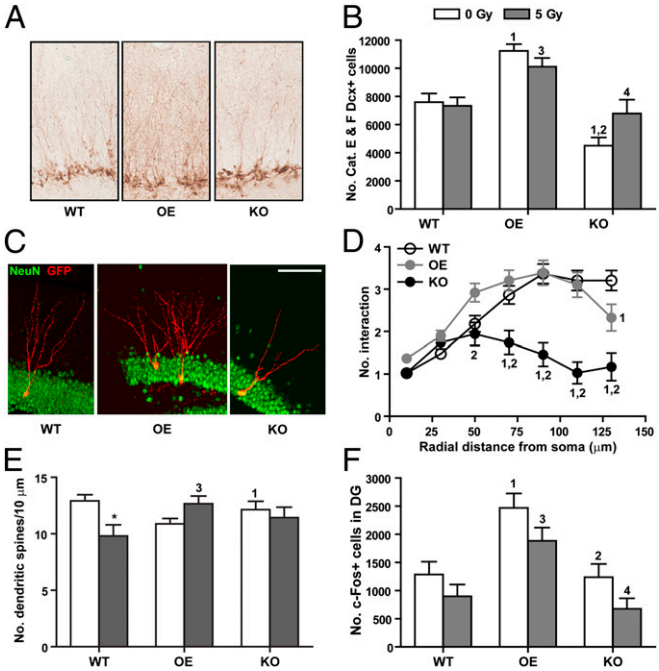

Fig. 3. Dendritic system affected by EC-SOD levels and irradiation. (*A*) Representative immunohistochemical images showing the soma and the dendritic network of Dcx$^+$ cells. (*B*) Total number of categories E and F Dcx$^+$ cells (Dcx$^+$ cells with more elaborate dendritic network). There was a significant interaction between genotype and treatment [$F_{(2,25)}$ = 3.53, P = 0.0445]. Genotype also played a significant role in the data variation [$F_{(2,25)}$ = 29.47, $P < 0.0001$]. (*C*) Representative images of dendritic arborizations in newly born neurons (labeled with GFP and NeuN). (Scale bar, 100 μm.) (*D*) Examination of the complexity of dendritic network by Sholl analysis. $n = 44$ (from three mice), 49 (from five mice), and 35 (from four mice) GFP$^+$ cells for WT, OE, and KO, respectively. (*E*) Dendritic spine densities following behavioral studies (see experimental timeline in Fig. 1*A*). n = 6–8 mice each. There was a significant interaction between genotype and treatment [$F_{(2,34)}$ = 5.81, P = 0.0068]. (*F*) Total number of c-Fos$^+$ cells in the hippocampal dentate gyrus. n = 5–8 mice each. Both irradiation [$F_{(1,27)}$ = 7.10, P = 0.0128] and genotype [$F_{(2,27)}$ = 6.42, $P < 0.0001$] played a significant role in the data variation. All data are presented as mean ± SEM. Two-way ANOVA (*B*, *E*, and *F*) and two-way repeated-measures ANOVA (*D*) with Bonferroni posttest were used for data analysis. *$P < 0.05$ compared with the sham-irradiated counterpart; 1, $P < 0.05$ compared with WT/0 Gy; 2, $P < 0.05$ compared with OE/0 Gy; 3, $P < 0.05$ compared with WT/5 Gy; 4, $P < 0.05$ compared with OE/5 Gy.

To determine if alterations in the dendritic complexity was associated with changes in neuronal activity, expression of the immediate early gene c-Fos was determined 2 mo following irradiation (see timeline in Fig. 2*A*). Sham-irradiated OE mice had significantly higher numbers of c-Fos$^+$ granule cells in the dentate gyrus (Fig. 3*F*). Irradiation resulted in reductions in c-Fos$^+$ cells across all genotypes; however, because of large biological variations the extent of reduction did not reach a statistically significant level. Total number of c-Fos$^+$ cells in irradiated OE mice remained significantly higher than that in irradiated WT and KO mice (Fig. 3*F*). Results from quantitative RT-PCR (qRT-PCR) analysis of c-Fos message levels in the hippocampal formation were consistent with the profile of c-Fos$^+$ cells among different cohorts (Fig. S6*A*).

EC-SOD and Irradiation Affect Expression of Neurotrophic Factors and Molecules Controlling Axon/Dendrite Maintenance. To identify the molecular and biochemical pathways involved in alterations in neurogenesis, dendritic arborization, and spine density because of differences in EC-SOD levels or as a result of radiation treatment, gene array studies were performed. Based on identified candidate genes associated with neurogenesis and neuroplasticity, qRT-PCR (Table S2) and Western blot analyses were then carried out. Two neurotrophic factors, brain-derived neurotrophic factor (Bdnf) and neurotrophin 3 (Ntf3), showed expression profiles that were favorable to OE mice in terms of long-term survival of newborn neurons and improved neuronal plasticity: (*i*) irradiated OE mice were able to maintain the same level of Bdnf expression when more than 30% reduction was observed in WT (t = 3.63, $P < 0.01$) and KO (t = 4.97, $P < 0.001$) mice following irradiation (Fig. 4*A*); (*ii*) expression levels of Ntf3 were significantly increased in irradiated OE (55% increase, t = 2.99, $P < 0.05$), but stayed the same in irradiated WT and KO mice (Fig. 4*B*).

Because activated/phosphorylated cAMP-response element binding protein (pCREB) is known to be associated with Bdnf and Ntf3 and is important for learning and memory (24–27), the level of pCREB was also determined. A significant reduction in pCREB was observed in irradiated WT mice (80% reduction, t = 2.62, $P <$ 0.05), implying a diminished level of pCREB-mediated neuronal function in this cohort. In contrast, no significant changes were identified in irradiated OE and KO mice. A similar profile was observed in the expression of the axon guidance molecule semaphorin 3C (Sema3C) with a significant reduction in irradiated WT (31% reduction, t = 2.97, $P < 0.05$) (Fig. 4*D*). Collectively, the data implicated a change in neurotrophic factors and guidance molecules with negative impact on neurogenesis and maintenance of the dendritic system in irradiated WT mice.

Ephrin A5 (Efna5), a ligand for the Eph-related tyrosine kinase receptor, and the nuclear receptor related protein 1 (Nurr1) were also differentially regulated by EC-SOD and irradiation: Efna5 expression levels were significantly elevated in irradiated KO (65% increase, t = 4.67, $P < 0.001$), but the levels were either not changed or reduced in irradiated WT and OE mice (Fig. 4*E*). Similarly, Nurr1 expression levels were significantly increased in irradiated KO mice (54% increase, t = 3.98, $P < 0.001$), but remained unchanged in WT and OE mice following irradiation (Fig. 4*F*). Other neurogenesis-related genes differentially regulated in irradiated KO mice include nNOS, Etv1, and Bcl2l1 (Fig. S6 *B–D*).

Discussion

In this study, we showed that: (*i*) EC-SOD deficiency had a negative impact on progenitor cell proliferation and long-term survival of newborn neurons in the dentate gyrus of hippocampus; (*ii*) high levels of EC-SOD in granule cells supported dendritic development and long-term survival of newborn neurons; (*iii*) compared with WT mice, OE and KO mice were less sensitive to irradiation-induced changes in hippocampal neurogenesis and the associated cognitive functions; and (*iv*) neurotrophic factors and molecules controlling axon/dendrite maintenance were differentially affected by EC-SOD levels and by irradiation.

Hippocampal neurogenesis and synaptic activities can be influenced by redox balance in the local microenvironment. Although EC-SOD is secreted into the extracellular environment, the enzyme is bound locally to extracellular matrix and only a small percentage is released as a circulating form in the CNS (17, 28). Therefore, by reconstituting EC-SOD expression to only mature neurons, we are able to generate a mouse model (OE mice) in which an EC-SOD–deficient SGZ is adjacent to an EC-SOD–rich granule cell layer in the hippocampal dentate gyrus (Fig. S7*A*). The manipulation did not result in changes in other SODs and major peroxidases in the hippocampal formation of OE mice (Fig. S7*B*).

Comparing the "hybrid" environment in OE mice to that with ubiquitous EC-SOD expression in WT or ubiquitous deficiency in KO mice, we showed that proliferation of neuronal progenitor cells was suppressed to the same extent in sham irradiated OE and KO mice (Fig. 2*H*), suggesting a negative effect of the EC-SOD–deficient neurogenic environment on progenitor cell proliferation. Moreover, because a small percentage of EC-SOD is expected to

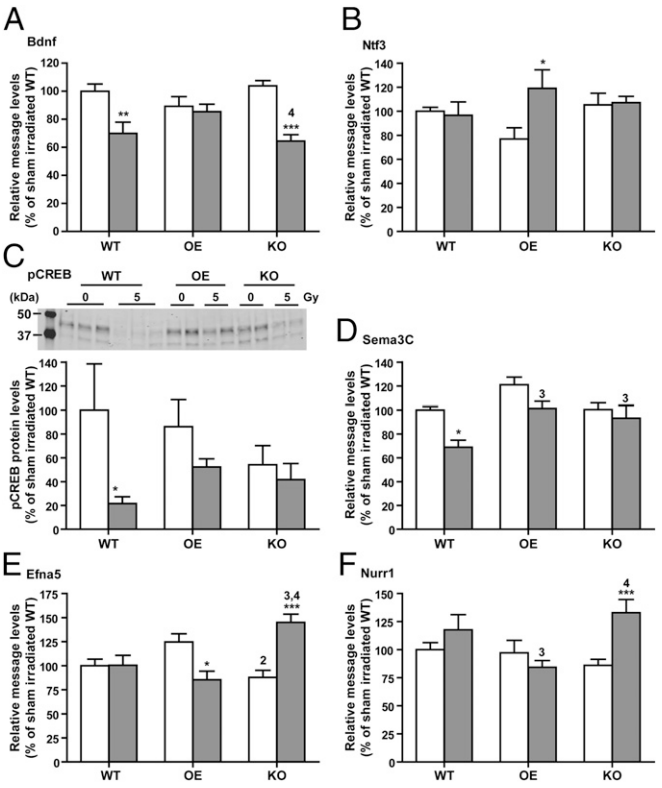

Fig. 4. Neurotrophic factors, axon/dendrite guidance, and transcription factors affected by EC-SOD and irradiation. (*A* and *B*) Relative message levels of Bdnf and Ntf3, respectively in the hippocampus. (*C*) pCREB protein levels in the hippocampus. (*D–F*) Relative message levels of Sema3C, Efna5, and Nurr1, respectively in the hippocampus. n = 8–15 mice each for message quantification; n = 5–10 each for pCREB analysis. All data are presented as mean ± SEM. All message levels were normalized to that of sham irradiated WT controls. Two-way ANOVA with Bonferroni posttest was carried out. *$P < 0.05$; **$P < 0.01$; ***$P < 0.001$ for comparison between 0 and 5 Gy within each genotype. 2, $P < 0.05$ compared with OE/0 Gy; 3, $P < 0.05$ compared with WT/5 Gy; 4, $P < 0.05$ compared with OE/5 Gy.

be released from granule cells and diffuse into the SGZ in OE mice, it is reasonable to expect low levels of EC-SOD in the neurogenic environment in OE mice (17). Consequently, the data imply that to maintain normal progenitor cell proliferation, it may be critical for neuronal progenitor cells per se to produce EC-SOD. The number of immature neurons (Dcx^+ cell) in sham-irradiated OE and KO mice showed a similar profiles to that of $BrdU^+$ numbers (Fig. 2*I*), suggesting that EC-SOD deficiency did not affect the initial differentiation toward the neuronal lineage and that the low number of Dcx^+ cells in sham-irradiated OE and KO mice probably stemmed from changes in the proliferation of neuronal progenitor cells.

There appeared to be a positive association between EC-SOD levels in the granule cell layer and the number of immature neurons with more elaborate dendritic development, which was also reflected in mature newborn neurons with more extensive dendritic arborization (Fig. 3 *A–D*). The elaborate dendritic system likely provided more synaptic connections that had been reported to be important for the survival and functional integration of newborn neurons (29). Consequently, the extent of neuronal activity, based on the number of c-Fos^+ cells in the dentate gyrus, was significantly higher in sham-irradiated OE mice compared with sham-irradiated WT and KO mice (Fig. 3*F*). It was possible that the redox environment in the EC-SOD–rich granule cell layer promoted dendritic development in newborn neurons in OE mice. How this was accomplished was not entirely clear. EC-SOD had been shown to control the bioavailability of nitric oxide (NO) within the vascular wall and the lung (30, 31). Although similar work had not been performed in the nervous system, it was reasonable to assume that more NO would be available in the OE mice to facilitate dendrite outgrowth (32, 33). Because the molecular layer of dentate gyrus was expected to be devoid of EC-SOD (other than the circulating form originating from the granule cells) in OE mice, the observation that the dendrites in OE mice did not reach as far into the molecular layer as that in WT mice (Fig. 3 *C* and *D*) also supported a role of EC-SOD in dendritic arborization and maintenance.

Sham-irradiated OE mice appeared to make more mistakes in the beginning of RAWM training and were not able to discern novel placement of an object in the NLR tests (Fig. 1 *B* and *D*, and Fig. S1). It was possible that the more elaborate dendritic network in OE mice resulted in more synaptic connections that were not necessarily beneficial for synaptic transmission. Alternatively, an earlier study using an independent strain of transgenic mice with ubiquitous overexpression of EC-SOD showed similar cognitive deficits and suggested that normal levels of superoxide radicals may be important for hippocampal-dependent learning and that high levels of EC-SOD can affect learning by reducing extracellular superoxide needed for NMDA receptor activation (34).

Dendritic arborization and integration into the existing network are tightly linked to the survival of newborn neurons (29). Although increased dendritic arborization did not affect long-term survival of newborn neurons in sham-irradiated OE mice, reduced dendritic networks in sham-irradiated KO mice (Fig. 3 *C* and *D*) may be, in part, responsible for reduced long-term survival of newborn neurons. Thus, comparison between the number of newborn neurons ($BrdU^+/NeuN^+$ cells) (Fig. 2*E*) and the number of immature neurons (Dcx^+ cells) (Fig. 2*I*) showed that, whereas 6% and 6.6% immature neurons in WT and OE mice, respectively, became mature neurons 4 wk later, only 3.1% in KO mice made it that far (Table S1). The defect in KO mice was not just limited to the hippocampus because behavioral studies showed learning deficits in sham-irradiated KO mice in the hippocampal-independent NOR task as well (Fig. 1 *B* and *E*, and Fig. S1).

Following a single dose of cranial irradiation, hippocampal neurogenesis in WT mice decreased by 50%, but no significant reduction was observed in irradiated OE or KO mice (Fig. 2 *B* and *C*). Consequently, the percentage of immature neurons that became mature remained at 3% in irradiated KO mice, but it went from 6% to 3.5% in irradiated WT mice. Interestingly, the survival was enhanced to 9.2% in irradiated OE mice (Table S1). This result may be partly because of enhanced expression of Ntf3 and the ability to maintain normal levels of Bdnf expression in the post-irradiation environment in OE mice (Fig. 4 *A* and *B*). Together with normal pCREB activation (Fig. 4*C*) and normal dendritic spine density (Fig. 3*E*), the data were consistent with the observation that irradiated OE mice were able to maintain the same performance level in the RAWM task and improve in the NLR task (Fig. 1 *B* and *D*).

Although no reduction in neurogenesis was seen in irradiated KO mice, the number of newborn neurons remained low compared with irradiated WT and OE mice. However, irradiated KO mice were able to improve performance in the RAWM task (Fig. 1*B*). The dissociation between neurogenesis and cognitive performance in this cohort suggested that factors other than neurogenesis probably played a prominent role. We showed that irradiated KO mice were able to maintain normal dendritic spine density (Fig. 3*E*), which was important for normal synaptic transmission. In addition, irradiated KO mice were able to maintain normal Sema3C expression and up-regulate Efna5 and Nurr1 (Fig. 4 *D–F*). Sema3C had been shown to be important for axon guidance and neuritogenesis (35, 36); Efna5 was shown to enhance survival of adult born neurons and increase normal synaptic transmission in the hippocampus (37); and Nurr1 expression was important for

normal cognitive processes (38, 39). Collectively, the transcriptional profile would have supported a more robust cognitive learning in irradiated KO mice. How irradiated KO mice maintained Sema3C and up-regulated Efna5 and Nurr1 expression in the hippocampus was not clear, but some of these messages may be regulated by pCREB through activation of the redox-sensitive ERK1/2 (40, 41).

Taking these data together, it is possible that normal cognitive performance in irradiated OE and KO mice are supported by different mechanisms with the OE environment maintained by neurotrophic factors and the downstream pCREB signaling pathway and the KO environment enhanced by dendritic maintenance and cognitive processes to support survival of newborn neurons and normal cognitive learning. Additionally, the study results revealed the importance of EC-SOD in neuronal progenitor cell proliferation, dendritic development, and protection against irradiation. In the future, it will be reasonable to test, individually and in combination of, small synthetic molecules with SOD-like property or with an ability to mimic the function of neurotrophic factors to provide an environment that supports all stages of hippocampal neurogenesis and synaptic connections to preserve neurocognitive functions following cranial irradiation.

Methods

Mouse models used in the study have been described (13, 17). Neurogenesis and behavioral studies follow previously established procedures (13, 15, 16). Detailed descriptions for all experimental procedures are provided in *SI Methods*.

ACKNOWLEDGMENTS. We thank Xinli Wang for excellent animal care; Sunny Jeong for technical assistance; the Stanford Neuroscience Gene Vector and Virus Core (supported by National Institute of Neurological Disorders and Stroke P30 NS069375) for producing the MLV-CAG-GFP used in this study; and Drs. Stefan Marklund and James Crapo for making extracellular-superoxide dismutase KO mice available. This work was supported by funding from the National Institutes of Health Grants NS046051 and NS072143 (to J.R.F. and D.J.C.); a Veteran's Affairs Merit review (T.-T.H.); a Department of Neurology and Neurological Sciences start-up fund (to T.-T.H.); a Palo Alto Institute for Research and Education residual fund (to T.-T.H.); and the resources and facilities at the Veteran's Affairs Palo Alto Health Care System.

1. Laack NN, Brown PD (2004) Cognitive sequelae of brain radiation in adults. *Semin Oncol* 31(5):702–713.
2. Sarkissian V (2005) The sequelae of cranial irradiation on human cognition. *Neurosci Lett* 382(1-2):118–123.
3. Gondi V, Tomé WA, Mehta MP (2010) Why avoid the hippocampus? A comprehensive review. *Radiother Oncol* 97(3):370–376.
4. Bovi JA, White J (2012) Radiation therapy in the prevention of brain metastases. *Curr Oncol Rep* 14(1):55–62.
5. Mizumatsu S, et al. (2003) Extreme sensitivity of adult neurogenesis to low doses of X-irradiation. *Cancer Res* 63(14):4021–4027.
6. Raber J, et al. (2004) Radiation-induced cognitive impairments are associated with changes in indicators of hippocampal neurogenesis. *Radiat Res* 162(1):39–47.
7. Kim JS, et al. (2012) Comparison of the dose-response relationship of radiation-induced apoptosis in the hippocampal dentate gyrus and intestinal crypt of adult mice. *Radiat Prot Dosimetry* 148(4):492–497.
8. Motomura K, Ogura M, Natsume A, Yokoyama H, Wakabayashi T (2010) A free-radical scavenger protects the neural progenitor cells in the dentate subgranular zone of the hippocampus from cell death after X-irradiation. *Neurosci Lett* 485(1):65–70.
9. Quik EH, et al. (2012) Reduced growth hormone secretion after cranial irradiation contributes to neurocognitive dysfunction. *Growth Horm IGF Res* 22(1):42–47.
10. Quik EH, et al. (2012) Cognitive performance in older males is associated with growth hormone secretion. *Neurobiol Aging* 33(3):582–587.
11. Riley PA (1994) Free radicals in biology: Oxidative stress and the effects of ionizing radiation. *Int J Radiat Biol* 65(1):27–33.
12. Panagiotakos G, et al. (2007) Long-term impact of radiation on the stem cell and oligodendrocyte precursors in the brain. *PLoS ONE* 2(7):e588.
13. Rola R, et al. (2007) Lack of extracellular superoxide dismutase (EC-SOD) in the microenvironment impacts radiation-induced changes in neurogenesis. *Free Radic Biol Med* 42(8):1133–1145, discussion 1131–1132.
14. Greenberger JS, Epperly MW (2007) Review. Antioxidant gene therapeutic approaches to normal tissue radioprotection and tumor radiosensitization. *In Vivo* 21(2):141–146.
15. Monje ML, Mizumatsu S, Fike JR, Palmer TD (2002) Irradiation induces neural precursor-cell dysfunction. *Nat Med* 8(9):955–962.
16. Raber J, et al. (2011) Irradiation enhances hippocampus-dependent cognition in mice deficient in extracellular superoxide dismutase. *Hippocampus* 21(1):72–80.
17. Zou Y, Chen CH, Fike JR, Huang TT (2009) A new mouse model for temporal- and tissue-specific control of extracellular superoxide dismutase. *Genesis* 47(3):142–154.
18. Deng W, Aimone JB, Gage FH (2010) New neurons and new memories: How does adult hippocampal neurogenesis affect learning and memory? *Nat Rev Neurosci* 11(5):339–350.
19. Barker GR, Warburton EC (2011) When is the hippocampus involved in recognition memory? *J Neurosci* 31(29):10721–10731.
20. Biscaro B, Lindvall O, Tesco G, Ekdahl CT, Nitsch RM (2012) Inhibition of microglial activation protects hippocampal neurogenesis and improves cognitive deficits in a transgenic mouse model for Alzheimer's disease. *Neurodegener Dis* 9(4):187–198.
21. Ekdahl CT (2012) Microglial activation—Tuning and pruning adult neurogenesis. *Front Pharmacol* 3:41.
22. Thored P, et al. (2009) Long-term accumulation of microglia with proneurogenic phenotype concomitant with persistent neurogenesis in adult subventricular zone after stroke. *Glia* 57(8):835–849.
23. Plümpe T, et al. (2006) Variability of doublecortin-associated dendrite maturation in adult hippocampal neurogenesis is independent of the regulation of precursor cell proliferation. *BMC Neurosci* 7:77.
24. Bender RA, Lauterborn JC, Gall CM, Cariaga W, Baram TZ (2001) Enhanced CREB phosphorylation in immature dentate gyrus granule cells precedes neurotrophin expression and indicates a specific role of CREB in granule cell differentiation. *Eur J Neurosci* 13(4):679–686.
25. Jagasia R, et al. (2009) GABA-cAMP response element-binding protein signaling regulates maturation and survival of newly generated neurons in the adult hippocampus. *J Neurosci* 29(25):7966–7977.
26. Merz K, Herold S, Lie DC (2011) CREB in adult neurogenesis—Master and partner in the development of adult-born neurons? *Eur J Neurosci* 33(6):1078–1086.
27. Herold S, Jagasia R, Merz K, Wassmer K, Lie DC (2011) CREB signalling regulates early survival, neuronal gene expression and morphological development in adult subventricular zone neurogenesis. *Mol Cell Neurosci* 46(1):79–88.
28. Karlsson K, Sandström J, Edlund A, Marklund SL (1994) Turnover of extracellular-superoxide dismutase in tissues. *Lab Invest* 70(5):705–710.
29. Bergami M, Berninger B (2012) A fight for survival: The challenges faced by a newborn neuron integrating in the adult hippocampus. *Dev Neurobiol* 72(7):1016–1031.
30. Jung O, et al. (2003) Extracellular superoxide dismutase is a major determinant of nitric oxide bioavailability: In vivo and ex vivo evidence from ecSOD-deficient mice. *Circ Res* 93(7):622–629.
31. Ahmed MN, Codipilly C, Hogg N, Auten RL (2011) The protective effect of overexpression of extracellular superoxide dismutase on nitric oxide bioavailability in the lung after exposure to hyperoxia stress. *Exp Lung Res* 37(1):10–17.
32. Chen J, et al. (2006) N-cadherin mediates nitric oxide-induced neurogenesis in young and retired breeder neurospheres. *Neuroscience* 140(2):377–388.
33. Morales-Medina JC, Mejorada A, Romero-Curiel A, Flores G (2007) Alterations in dendritic morphology of hippocampal neurons in adult rats after neonatal administration of N-omega-nitro-L-arginine. *Synapse* 61(9):785–789.
34. Thiels E, et al. (2000) Impairment of long-term potentiation and associative memory in mice that overexpress extracellular superoxide dismutase. *J Neurosci* 20(20):7631–7639.
35. Moreno-Flores MT, et al. (2003) Semaphorin 3C preserves survival and induces neuritogenesis of cerebellar granule neurons in culture. *J Neurochem* 87(4):879–890.
36. Steup A, et al. (2000) Sema3C and netrin-1 differentially affect axon growth in the hippocampal formation. *Mol Cell Neurosci* 15(2):141–155.
37. Hara Y, Nomura T, Yoshizaki K, Frisén J, Osumi N (2010) Impaired hippocampal neurogenesis and vascular formation in ephrin-A5-deficient mice. *Stem Cells* 28(5):974–983.
38. Colón-Cesario WI, et al. (2006) Knockdown of Nurr1 in the rat hippocampus: Implications to spatial discrimination learning and memory. *Learn Mem* 13(6):734–744.
39. Peña de Ortiz S, Maldonado-Vlaar CS, Carrasquillo Y (2000) Hippocampal expression of the orphan nuclear receptor gene hzf-3/nurr1 during spatial discrimination learning. *Neurobiol Learn Mem* 74(2):161–178.
40. Kim SY, et al. (2006) The dopamine D2 receptor regulates the development of dopaminergic neurons via extracellular signal-regulated kinase and Nurr1 activation. *J Neurosci* 26(17):4567–4576.
41. Darragh J, et al. (2005) MSKs are required for the transcription of the nuclear orphan receptors Nur77, Nurr1 and Nor1 downstream of MAPK signalling. *Biochem J* 390 (Pt 3):749–759.

Supporting Information

Zou et al. 10.1073/pnas.1216913110

SI Methods

Animals. Generation of TRE-*Sod3*-GFP transgenic (1) and extracellular-superoxide dismutase (EC-SOD) knockout mice (*Sod3*$^{-/-}$) (2) has been described; CamKII-tTA transgenic mice (3) were initially obtained from the Jackson Laboratory (stock no. 007004). All three mouse strains were maintained on the C57BL/6J background. To generate TRE-*Sod3*-GFP and CamKII-tTA double-transgenic mice on the EC-SOD–null background, each transgenic line was crossed to EC-SOD KO in two successive rounds of breeding to generate TRE-*Sod3*-GFP/KO and CamKII-tTA/KO mice. The absence of endogenous EC-SOD protein in TRE-*Sod3*-GFP/KO and CamKII-tTA/KO mice was verified by Western blot analysis of mouse serum (1). Crosses between TRE-*Sod3*-GFP/KO and CamKII-tTA/KO mice generated TRE-*Sod3*-GFP/CamKII-tTA double-transgenic mice on the EC-SOD null background and the mice were designated as overexpressors (OE) in this study. EC-SOD knockout mice were generated from the same breeding as littermates and were designated as KO. Because the breeding could not provide WT controls, C57BL/6J mice were generated in parallel in the same housing area and were designated as WT. All mice were kept in a barrier facility with a 12-h dark-light cycle, given food and water ad libitum, and maintained in microisolators with a constant temperature between 20 °C and 26 °C. All animal procedures were reviewed and approved by the Subcommittee on Animal Studies (National Institutes of Health assurance number A3088-01) at the Veteran's Affairs Palo Alto Health Care System and in accordance with the Public Health Service Policy on Humane Care and Use of Laboratory Animals.

All transgenic and KO mice were identified by PCR genotyping. TRE-*Sod3*-GFP and CamKII-tTA mice were genotyped as previously described (1) and EC-SOD KO mice were genotyped with the following primers: (forward) 5′-GTT TCC ACC CAA TGT CGA GC-3′ and (reverse) 5′-CCA GTC ATA GCC GAA TAG CC-3′ primers for the KO allele; (forward) 5′-GCA ATC TGC AGG GTA CAA CC-3′ and (reverse) 5′-TCT TGC GCT CCT TTG TCT GG-3′ primers for the WT allele. PCR products for the WT and KO allele were ∼500 bp and 300 bp, respectively. Because of the high GC content in EC-SOD sequence, 40% (vol/vol) DMSO was included in the 10× PCR buffer [200 mM Tris, PH 9.0, 160 mM $(NH_4)_2SO_4$] and the reaction was carried out for 35 cycles (94 °C for 30 s, 60 °C for 30 s, and 72 °C for 30 s).

Cranial Irradiation. Two-mo-old male WT, KO, and OE mice were anesthetized (intraperitoneal injection, 120 mg/kg ketamine, and 5 mg/kg xylazine) and sham-irradiated or irradiated with a single dose of 5 Gy using a Mark 1 Cesium Irradiator (J. L. Shepherd and Associates) with an dose rate of 71.4 cGy/min. Details of irradiation set up has been described previously (4, 5), with the mouse body shielded with a minimum of 5-cm lead in all directions and the head exposed to the source of the irradiator through the opening of the lead shield. Radiation dose was monitored by placing the InLight nanoDot (Landauer) dosimeter in the mouse holder at the location of the mouse head.

Behavioral Tests. Before the behavioral tests, each mouse was habituated to handling by laboratory personnel for 1–2 min each day for 7 d. All behavioral studies were captured by a digital camera and the study results analyzed by TopScan Lite (Cleversys) or by hand. Each experimental group included 17–20 animals. All animals received sham or cranial irradiation at 2 mo of age, and behavior studies were commenced 1 mo following irradiation (Fig. 1*A*). Behavioral tests were carried out in the following order: open field, novel location recognition (NLR) and novel object recognition (NOR), elevated zero maze, and radial-arm water maze (RAWM). A separate set of mice were used for the assessment of tactile and heat sensitivities.

Open field. The open-field arenas were constructed with white opaque high-density polyethylene plastic and each measured 45 × 45 × 45 cm. The entire box was wiped with 70% (vol/vol) alcohol between each test subject. Each mouse was placed into the arena from the middle of the south wall under dim light and allowed to explore the box for 10 min. Overall activities and the time spent in the center vs. the outer 50% area were determined for each mouse. The time spent in the center 50% area was used as an index of general anxiety levels.

Novel location and novel object recognition. NLR and NOR tasks were carried out in the same arenas as that used for the open field test. A large visual cue was placed on the north wall of the arena, and mice were always placed into the arena from the middle of the south wall. One day after the open field test, each mouse was left in the arena with two identical objects (OBJ1 and OBJ2, made of Lego blocks) for 10 min for habituation. The two identical objects were placed side by side with equal distance from the east and west walls and were 30 cm away from the visual cue (i.e., the north wall). The next day, mice were first given three 10-min trials with identical setting from the day before. The time spent exploring the two objects was recorded. In the fourth 10-min trial, OBJ1 was moved toward the visual cue (novel location), and the time spent exploring OBJ1 in the new location was recorded. In the fifth 10-min trail, OBJ2 (the familiar object) was replaced by a new object of different shape and color (OBJ3, novel object), and the time spent exploring OBJ3 was recorded. The intertrial intervals were 5 min and mice were returned to their home cage during that time. Objects were replaced with replicates after each trial, and 4% (vol/vol) acetic acid was used to clean and remove potential odors. Exploration behavior in the first 5 min was used to assess location (trial 4) and object (trial 5) recognition. The data were calculated as exploration ratio for and as time (in seconds) spent exploring OBJ1 in the novel location (in trial 4) vs. that for exploring OBJ2 in its original location (in trial 4) in NLR. Exploration ratio for and time spent exploring the novel object (OBJ3) vs. that for exploring the familiar object (OBJ1) in trial 5 were calculated for novel object recognition. Exploration ratio for novel and familiar location/object was calculated as *T*novel/(*T*novel + *T*familiar) and *T*familiar/(*T*novel + *T*familiar), respectively, where *T* equals time, as previously described (6).

Elevated zero maze. The elevated zero maze was constructed based on a published design (7) with an outer diameter of 24 inches and inner diameter of 20 inches, and sits 24 inches above the floor. Walls in the closed quadrants are 6 inches tall. Mice were placed facing the closed quadrant 1 of the elevated zero maze to begin the 5-min test period. The latency to enter an open quadrant, total time spent in open and closed quadrants, time in each of the four quadrants, and the activity in closed quadrants were recorded. Distance traveled and the number of fecal boli at the end of each test was also calculated. Several of these measurements were used to determine general anxiety. After mice were tested, the chamber was cleaned with 70% ethanol and allowed to dry.

Radial-arm water maze. RAWM is a hippocampus-dependent task that has been described at length in previous publications (8, 9). Mice received a total of 15 trials on each of the training and test day, including two 30-min breaks following trials 6 and 12. During the break period, the mice were returned to their home cages. On the first day (training day), trials 1–12 alternated between visible and hidden platforms, and trials 13–15 used hidden platform only.

On the second day (test day), mice were given 15 trials of hidden-platform test in the RAWM to assess their memory for the hidden-platform location. Spatial learning and memory was measured by counting the number of arm entry errors that mice made on each trial. An arm entry error was operationally defined as entering one of the arms that did not contain either the visible or the hidden platform. Average arm entry errors were calculated for blocks of three trials.

Tactile sensitivity. Tactile sensitivity was measured by using von Frey filaments following the "up-down" method described by Chaplan et al. (10), Sahbaie et al. (11), and DeLorey et al. (12). After acclimating mice on wire mesh platforms inside clear cylindrical plastic enclosures (10-cm diameter, 40-cm height), fibers of sequentially increasing stiffness were applied to the plantar aspect of the hind paw. The fiber was pressed and left in place for 5 s, and hind paw withdrawal was scored as a response. After the initial response, four fibers were applied as follows to confirm the paw withdrawal threshold: a less stiff fiber was applied; when no response was obtained, the next stiffest fiber in the series was applied to the same paw; if a response was obtained, a less stiff fiber was applied again. By using a data-fitting algorithm, the paw withdrawal threshold was calculated and subjected to parametric statistical analysis (13).

Heat sensitivity. Heat sensitivity was measured using the method described by Hargreaves and modified for mice (12, 14, 15). Mice were acclimated on a temperature controlled glass platform (23.5–24 °C) in the same plastic enclosures as the von Frey test. A radiant heat source and a timer were activated simultaneously with the heat source focused onto the mid plantar area of the hind paw. When the paw was withdrawn, both heat and timer were halted. Withdrawal latency of the paw from the heat source was measured. To prevent tissue damage, a 15-s cutoff was used. Three measurements were made per animal per test session.

BrdU Administration. To label proliferating cells, the thymidine analog BrdU (Sigma) was prepared in PBS and administered (50 mg/kg i.p.) once per day for 7 contiguous days or twice in 1 d with an 8-h interval. Animals were injected with BrdU 4 wk after irradiation and killed either 3 wk after the last BrdU injection of the 7-d protocol or 16 h after the second BrdU injection of the 1-d protocol (Fig. 2).

Tissue Processing. Mice were deeply anesthetized with ketamine and xylazine as described above and perfused intracardially with 0.9% NaCl. Brains were postfixed with 4% (wt/vol) PBS buffered paraformaldehyde for 48 h, and immersed in 30% (wt/vol) sucrose (in PBS) for cryoprotection. Forty-micrometer serial coronal sections encompassing the entire hippocampal formation were obtained with a sliding microtome (Leica SM 2000R, Leica). Free-floating brain sections were stored in 24-well plates at 4 °C in a cryoprotection solution containing 0.01 M NaH_2PO_4, 30% (vol/vol) glycerin, and 30% (vol/vol) ethylene glycol.

Immunohistochemical Staining. For the detection of BrdU, brain sections were washed in Tris-buffered Tween solution (TBST) and then treated with 0.6% hydrogen peroxide and 0.1% Triton X-100 at room temperature for 30 min. To denature DNA, sections were treated with 3 M hydrochloric acid (HCl) at 37 °C for 30 min. Sections were then incubated with a blocking solution containing 10% (vol/vol) rabbit serum in TBST for 1 h at room temperature, and then incubated with rat anti-BrdU (ab6326, 1:1,000 diluted in blocking solution; Abcam) overnight (about 16 h) followed by biotinylated secondary antibody (rabbit anti-rat IgG, BA-4000, 1:1,000; Vector Laboratories). For the detection of doublecortin (Dcx) and c-Fos, we omitted HCl treatment, and brain sections were incubated with goat anti-Dcx (sc-8066, 1:300; Santa Cruz Biotechnology) or rabbit anti–c-Fos (PC38, 1:20,000, EMD, Millipore) for 48 h at 4 °C followed by incubation with biotinylated secondary antibody at room temperature for 1 h. Sections were then treated with the ABC kit (PK-4000; Vector Laboratories), and diaminobenzidine (DAB, D5905; Sigma) was used to develop the signals. To determine the number of $BrdU^+/NeuN^+$ and $BrdU^+/GFAP^+$ cells in the subgranular zone (SGZ), immunofluorescence staining of BrdU/NeuN/GFAP was carried out. Brain sections were first rinsed in TBST and incubated in 3 M HCl to allow DNA denaturation. Sections were incubated simultaneously with rat anti-BrdU (1:1,000), mouse anti-NeuN (MAB377, 1:500; Chemicon), and rabbit anti-GFAP (Z0334, 1:1,000; Dako) in TBST containing 0.2% Triton X-100 (vol/vol) and 10% goat serum overnight (about 16 h) at 4 °C followed by incubation with secondary antibodies, Alexa 555 goat anti-rat IgG, Alexa 488 goat anti-mouse IgG, and Alexa 647 goat anti-rabbit IgG (all at 1:500 dilution; Invitrogen), at room temperature for 1 h. Sections were mounted with ProLong antifade (P36935; Invitrogen) solution and stored in −20 °C. One in every sixth sections of the entire hippocampal formation were used for BrdU staining and one in every 12th sections used for Dcx, c-Fos, and BrdU/NeuN/GFAP triple staining.

Cell Counting. The stereological counting principle of systematic, uniformly random sampling of sections (16) was applied to determine the total number of $BrdU^+$ and Dcx^+ cells in the SGZ, as well as c-Fos^+ cells in the granule cell layer, of hippocampal dentate gyrus. SGZ was defined as the ±16-μm zone along the border between the hilus and the granule cell layer. Any positively stained cells appearing at more than two times the nuclear diameter away from the border of granule cell layer were not considered. To avoid overestimation, only BrdU signals that can be identified as constituting the middle cross-section of a nucleus were counted. Spot-like patterns from small patches of chromatin/chromosome were not considered. The entire dentate gyrus (bilateral) of each brain section was photographed and the number of $BrdU^+$ cells in the SGZ was determined for each mouse. Total $BrdU^+$ cell counts were calculated by multiplying the initial counts by 6. Similar to BrdU analysis, Dcx^+ cells and Dcx^+ cells with a more mature appearance (i.e., category E and F Dcx^+ cells) (17) were counted in the SGZ. The total number of Dcx^+, mature Dcx^+ cells, and c-Fos^+ cells were calculated by multiplying the initial counts by 12.

Immunofluorescence stained sections were analyzed with a LSM 510 Confocal Laser Scanning Microscope (Carl Zeiss MicroImaging), with the detection pinhole set at 1 Airy Unit. *Z* sections were taken at 3-μm intervals. $BrdU^+$ cells were examined with split-panel analysis. Only those cells for which the $BrdU^+$ nucleus was unambiguously associated with the lineage-specific marker were scored as positive. For each lineage-specific marker, the percentage of $BrdU^+$ cells expressing that marker was determined. For most samples, at least 100 $BrdU^+$ cells were examined for lineage analysis. However, because KO mice had lower numbers of $BrdU^+$ cells, all $BrdU^+$ cells in every 12th sections were examined in the KO groups. Total number of lineage-specific $BrdU^+$ cells for each animal was then calculated by multiplying the percentage by the total number of $BrdU^+$ cells in the SGZ.

Activated Microglia. Total number of activated microglia was counted at the dorsal hippocampus level as described previously (18) with minor modifications. Rat anti-mouse CD68 monoclonal antibody (1:1,500, ab53444; Abcam) and biotinylated rabbit anti-rat IgG (1:200, BA-4001; Vector Laboratories) were used as the primary and secondary antibody, respectively. Staining signals were further amplified with an avidin/biotin amplification system (Vector Laboratories) followed by Cy3 tyramide amplification (PerkinElmer). Nuclei were counterstained with Cytox-Green (Invitrogen). Regions of interest containing the granular cell layer were selected using AxioImager imaging software (Zeiss) and the numbers of positive cells were counted within the selected area. To avoid overestimation, only intensely stained cell body with short, stout processes were counted. Eight coronally sectioned hippocampal dentate gyrus were examined for each mouse, and the final

results of activated microglia were expressed as number of cells per square millimeter.

Golgi Staining. A separate set of mice were used for Golgi staining and the procedure was carried out following behavioral studies. Golgi-Cox staining procedure was performed using the FD Rapid GolgiStain Kit (FD NeuroTechnologies). Coronal sections (100-μm thickness) were obtained with a Vibratome (VT1200S; Leica Microsystems) and were mounted on gelatin-coated slides. After color development, sections were examined with a Zeiss Imager D1 microscope, and images of dentate granular neurons were captured using an ORCA-ER digital camera (Hamamatsu Photonics). An investigator blinded to the genotype and treatment randomly selected dendrites (secondary and tertiary dendritic branches) from each mouse for quantification. Areas within 10 μm of the dendritic branch point or 10 μm of the dendritic terminals were excluded from analysis. Visible spines were counted in 10 dendritic segments (each 15–40 μm in length) from each mouse using ImageJ (National Institutes of Health). Only spines that were clearly protruding from the dendrites were counted, and they included two-headed, thin, and mushroom-shaped (19) spines. Spine density was expressed as average number of spines per 10-μm dendrite.

GFP Labeling of Newborn Neurons. GFP labeling of newborn neurons was carried out as described previously (20) using a retroviral vector MLV-CAG-GFP (21). High-titer MLV-CAG-GFP (1×10^8 units/mL) was injected stereotaxically into the dendate gyrus using the following coordinates: anterior-posterior (AP) = −2 mm from the bregma; lateral (LAT) = ± 1.6 mm; ventral (VENT) = 2.2 mm. Each site was injected with 0.5 μL retrovirus at a rate of 0.25 μL/min. Mice were killed 4 wk after injection to allow maturation of the newborn neurons. GFP-labeled cells were visualized with anti-GFP antibody (Invitrogen; A11122), and neurons were identified with NeuN antibody. The viral stock was produced by the Gene Vector and Virus Core facility at the Stanford Neuroscience Institute. Immunofluorescence stained sections were analyzed with a LSM 510 Confocal Laser Scanning Microscope (Carl Zeiss MicroImaging, Zeiss EC Plan-Neofluar, 20×/0.05) with the detection pinhole set at 1 Airy Unit. *Z* sections taken at 3-μm intervals were examined for GFP-labeled cells. The *z*-stack images of a single GFP^+ neuron were processed with ImageJ to obtain a stacked image. Dendrite tracing was then performed using the NeuronJ plugin. The traced images were used to determine the complexity of dendritic networks using the Advanced Sholl Analysis plugin. Dendritic lengths were obtained during the tracing process, and the number of branches was counted manually based on the traced image of GFP^+ neurons. Only GFP^+ cells with at least one dendrite (longer than the diameter of soma) were imaged and analyzed.

Western Blot Analyses. Protein levels of antioxidant enzymes, CuZn superoxide dismutase (CuZnSOD), Mn superoxide dismutase (MnSOD), EC-SOD, catalase, peroxiredoxin 1 (Prdx1), and peroxiredoxin 3 (Prdx3) in the hippocampus were determined by Western blot analysis using whole tissue homogenates. Fresh brains were dissected on ice and hippocampi were isolated, flash-frozen in liquid nitrogen, and stored at −80 °C. Hippocampal tissues from each animal were homogenized individually (weight to volume ratio 1:20) in T-PER buffer (Thermo Scientific), containing Complete protease inhibitor and phosphatase inhibitor (Roche). Homogenized samples were centrifuged at 10,000 × *g* at 4 °C for 5 min, and the supernatants were stored in 20-μL aliquots at −80 °C. Protein concentration of each sample was determined with a NanoVue spectrophotometer (GE Healthcare), and 50 μg of total proteins from each sample were used for Western blot analysis. Primary antibodies used in this study were described previously (18, 22). For quantification of the phosphorylated cAMP response element binding protein (pCREB, Ser133), nuclear extracts were used. Briefly, hippocampal tissues were treated with a hypotonic buffer (10 mM Hepes, 4 mM NaF, 10 μM Na_2MoO_4, 100 μM EDTA) to extract cytosolic proteins, followed by a nuclear extraction buffer [10 mM Hepes, 100 μM EDTA, 1.5 mM $MgCl_2$, 420 mM NaCl, 10% (vol/vol) glycerol, 1 mM DTT] to extract nuclear proteins. All buffers contained freshly prepared protease inhibitors and phosphatase inhibitors. Eighty micrograms of total nuclear proteins each were used for pCREB quantification (anti-pCREB, cat. No. 9198S, 1:1,000; Cell Signaling). IRDye-conjugated secondary antibodies were used for signal detection and quantification of all Western blot samples, and protein bands were visualized using an Odyssey Infrared Imaging System (Licor). Blots for antioxidant enzyme detections were reprobed with an antibody against β-actin (A3854, 1:50,000; Sigma) for normalization. pCREB signal intensities were normalized to the total DNA content of each sample.

Gene Expression Quantification by Quantitative PCR. Hippocampi were collected from individual mice, and RNA was extracted using TriZol reagent (Invitrogen) and reverse transcribed into cDNA using the SuperScript first strand synthesis kit (Invitrogen). Quantitative PCR (qPCR) was performed using the ABI 7900HT Sequence Detection System (Applied Biosystems) with SYBR Green PCR Master Mix (Applied Biosystems). Datapoints were calculated using standard curve methods and were expressed as the fold increase or decrease from the nonirradiated WT controls. The control value was set to 1.0, and GAPDH was used as an internal reference. Primers used for the qPCR analyses are listed in Table S2.

Statistical Analyses. Statistical analyses were carried out with GraphPad Prism 4.03 for Windows (GraphPad Software). One-way ANOVA with Tukey's posttest was carried out for comparison across multiple groups; two-way ANOVA with Bonferroni posttest was carried out to determine genotype × treatment interaction; and two-way repeated-measures ANOVA test was performed to compare the complexity of dendritic networks. Paired *t* test was carried out to compare results from RAWM (block 1 vs. block 10). Data tables for two-way ANOVA test were constructed in two different ways, with irradiation or genotype as the column factor, to allow postanalyses between 0 and 5 Gy within each genotype or analyses between WT, OE, and KO within each treatment group.

1. Zou Y, Chen CH, Fike JR, Huang TT (2009) A new mouse model for temporal- and tissue-specific control of extracellular superoxide dismutase. *Genesis* 47(3):142–154.
2. Carlsson LM, Jonsson J, Edlund T, Marklund SL (1995) Mice lacking extracellular superoxide dismutase are more sensitive to hyperoxia. *Proc Natl Acad Sci USA* 92(14): 6264–6268.
3. Mayford M, et al. (1996) Control of memory formation through regulated expression of a CaMKII transgene. *Science* 274(5293):1678–1683.
4. Acevedo SE, McGinnis G, Raber J (2008) Effects of 137Cs gamma irradiation on cognitive performance and measures of anxiety in Apoe-/- and wild-type female mice. *Radiat Res* 170(4):422–428.
5. Corniola R, Zou Y, Leu D, Fike JR, Huang TT (2012) Paradoxical relationship between Mn superoxide dismutase deficiency and radiation induced cognitive defects. *PLoS ONE* 7(11):e49367.
6. Mumby DG, Gaskin S, Glenn MJ, Schramek TE, Lehmann H (2002) Hippocampal damage and exploratory preferences in rats: memory for objects, places, and contexts. *Learn Mem* 9(2):49–57.
7. Shepherd JK, Grewal SS, Fletcher A, Bill DJ, Dourish CT (1994) Behavioural and pharmacological characterisation of the elevated "zero-maze" as an animal model of anxiety. *Psychopharmacology (Berl)* 116(1):56–64.
8. Alamed J, Wilcock DM, Diamond DM, Gordon MN, Morgan D (2006) Two-day radial-arm water maze learning and memory task; robust resolution of amyloid-related memory deficits in transgenic mice. *Nat Protoc* 1(4):1671–1679.
9. Villeda SA, et al. (2011) The ageing systemic milieu negatively regulates neurogenesis and cognitive function. *Nature* 477(7362):90–94.
10. Chaplan SR, Bach FW, Pogrel JW, Chung JM, Yaksh TL (1994) Quantitative assessment of tactile allodynia in the rat paw. *J Neurosci Methods* 53(1):55–63.

11. Sahbaie P, et al. (2009) Role of substance P signaling in enhanced nociceptive sensitization and local cytokine production after incision. *Pain* 145(3):341–349.
12. DeLorey TM, et al. (2011) Somatosensory and sensorimotor consequences associated with the heterozygous disruption of the autism candidate gene, Gabrb3. *Behav Brain Res* 216(1):36–45.
13. Poree LR, Guo TZ, Kingery WS, Maze M (1998) The analgesic potency of dexmedetomidine is enhanced after nerve injury: A possible role for peripheral alpha2-adrenoceptors. *Anesth Analg* 87(4):941–948.
14. Hargreaves K, Dubner R, Brown F, Flores C, Joris J (1988) A new and sensitive method for measuring thermal nociception in cutaneous hyperalgesia. *Pain* 32(1):77–88.
15. Li X, Angst MS, Clark JD (2001) A murine model of opioid-induced hyperalgesia. *Brain Res Mol Brain Res* 86(1-2):56–62.
16. West MJ (1999) Stereological methods for estimating the total number of neurons and synapses: Issues of precision and bias. *Trends Neurosci* 22(2):51–61.
17. Plümpe T, et al. (2006) Variability of doublecortin-associated dendrite maturation in adult hippocampal neurogenesis is independent of the regulation of precursor cell proliferation. *BMC Neurosci* 7:77.
18. Rola R, et al. (2007) Lack of extracellular superoxide dismutase (EC-SOD) in the microenvironment impacts radiation-induced changes in neurogenesis. *Free Radic Biol Med* 42(8):1133–1145, discussion 1131–1132.
19. Bourne JN, Harris KM (2008) Balancing structure and function at hippocampal dendritic spines. *Annu Rev Neurosci* 31:47–67.
20. Gu Y, Janoschka S, Ge S (2011) Studying the integration of adult-born neurons. *J Vis Exp*, (49):e2548.
21. Zhao C, Teng EM, Summers RG, Jr., Ming GL, Gage FH (2006) Distinct morphological stages of dentate granule neuron maturation in the adult mouse hippocampus. *J Neurosci* 26(1):3–11.
22. Kim A, et al. (2010) Enhanced expression of mitochondrial superoxide dismutase leads to prolonged in vivo cell cycle progression and up-regulation of mitochondrial thioredoxin. *Free Radic Biol Med* 48(11):1501–1512.

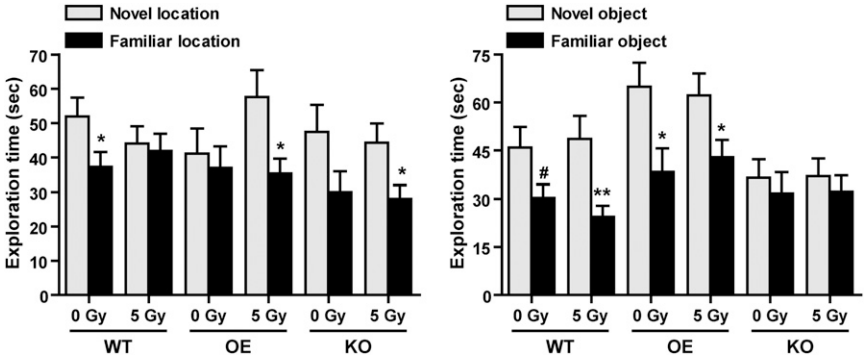

Fig. S1. Exploration time in NLR and NOR tests. Total exploration time (in seconds) was compared by Student *t* test between novel and familiar location/object within each cohort. $*P < 0.5$; $**P < 0.01$; $^{\#}P = 0.0533$. $n = 17–20$ mice per genotype per treatment.

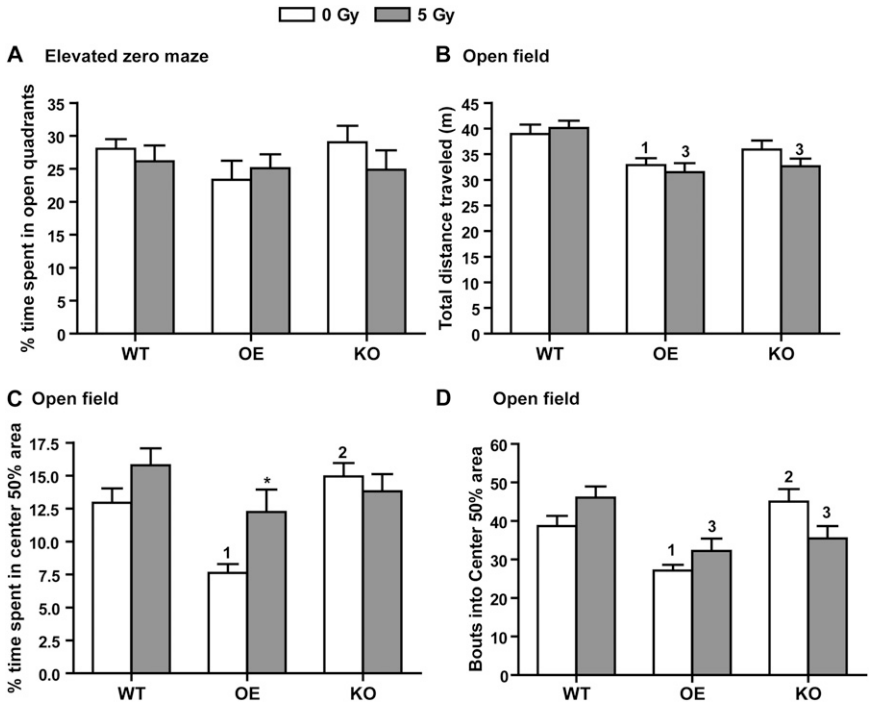

Fig. S2. Elevated zero maze and open field tests. (*A*) Results from elevated zero maze showing the average time spent in the two open quadrants during the 5-min testing period. (*B–D*) Results from open-field tests. (*B*) There was a small, but significant, reduction in total distance traveled in the open-field box in sham and irradiated OE mice. Irradiated KO mice also traveled a significantly shorter distance from irradiated WT controls. Only genotype [$F_{(2,106)} = 10.82$, $P < 0.0001$] contributed significantly to the data variation. (*C*) Sham-irradiated OE mice spent significantly less amount of time investigating the center 50% area of the open-field box. Irradiation [$F_{(1,106)} = 4.61$, $P = 0.0341$] and genotype [$F_{(2,106)} = 9.18$, $P = 0.0002$] both contributed significantly to the data variation. (*D*) Less time spent in the center 50% area in sham-irradiated OE mice was partly because of reduced entry into the open area. Bouts into the center 50% area in irradiated OE and KO mice were also significantly lower than that in irradiated WT mice. There was a significant interaction between treatment and genotype [$F_{(2,106)} = 5.23$, $P = 0.0068$]. Genotype [$F_{(2,106)} = 11.47$, $P < 0.0001$] also contributed significantly to the data variation. Data are presented as mean ± SEM. Two-way ANOVA with Bonferroni posttest was carried out. *$P < 0.05$ for comparison between 0 and 5 Gy within each genotype. 1, $P < 0.05$ compared with WT/0 Gy; 2, $P < 0.05$ compared with OE/0 Gy; 3, $P < 0.05$ compared with WT/5 Gy. n = 17–20 mice per genotype per treatment.

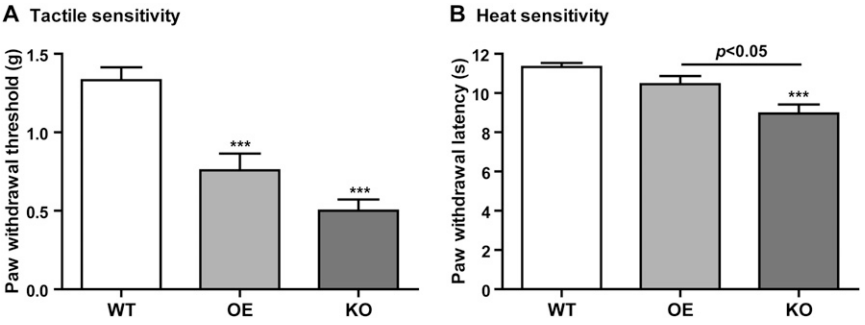

Fig. S3. Assessment of mechanical and heat sensitivity. Comparison of paw-withdrawal threshold after stimulation with von Frey filaments (*A*) and withdrawal latency to radiant heat (*B*). Data are presented as mean ± SEM and were analyzed by one-way ANOVA. Tactile sensitivity (*A*) $F_{(2,24)} = 23.4$, $P < 0.0001$; heat sensitivity (*B*), $F_{(2,24)} = 10.14$, $P = 0.0006$. Results from Bonferroni multiple comparison tests are presented on the bar graphs. ***$P < 0.001$ compared with WT mice. Data are presented as mean ± SEM. n = 9 mice each.

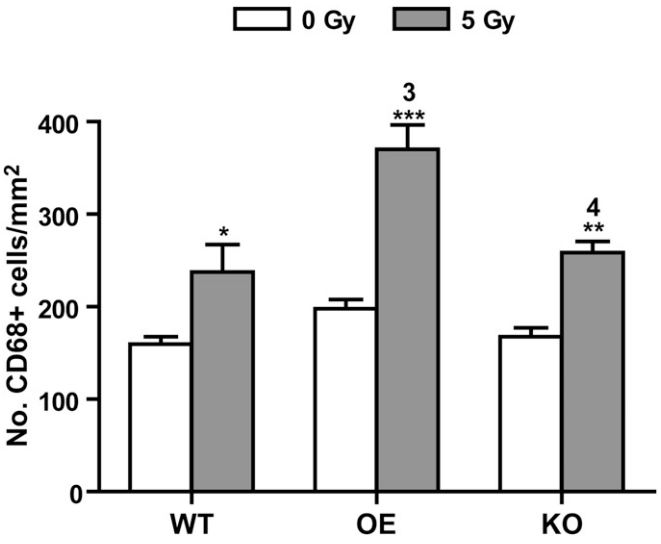

Fig. S4. Number of activated microglia in dorsal hippocampus. The number of $CD68^+$ cells in the hippocampal dentate gyrus was counted. Two-way ANOVA with Bonferroni posttest was carried out. Posttest results are presented on the graph: $*P < 0.05$, $**P < 0.01$, $***P < 0.001$ for comparison between 0 and 5 Gy within each genotype. 3, $P < 0.05$ compared with WT/5 Gy; 4, $P < 0.05$ compared with OE/5 Gy. There was a significant interaction between treatment and genotype [$F_{(2,24)} = 4.01$, $P = 0.0314$]. Irradiation [$F_{(1,24)} = 59.29$, $P < 0.0001$] and genotype [$F_{(2,24)} = 12.78$, $P = 0.0002$] also contributed significantly to the data variation. $n = 5$ mice per genotype per treatment. Data are presented as mean ± SEM.

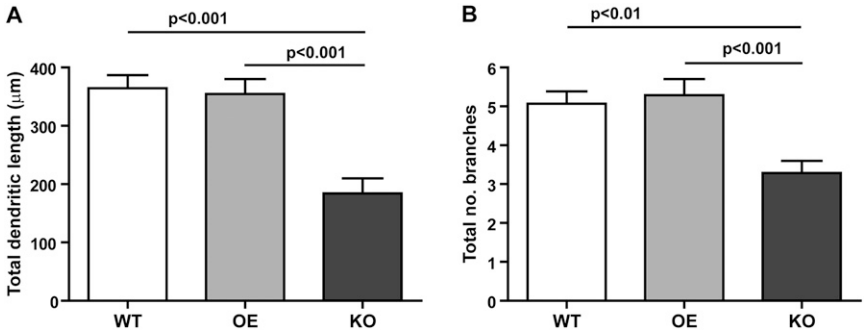

Fig. S5. Dendritic arborization of newborn neurons. Total dendritic length (*A*) and number of branches (*B*) were determined. Data were analyzed with one-way ANOVA with Tukey posttest. $n = 44$ (from three mice), 49 (from five mice), and 35 (from four mice) GFP^+ cells from WT, OE, and KO, respectively. Posttest results are shown on the graph. Data presented as mean ± SEM.

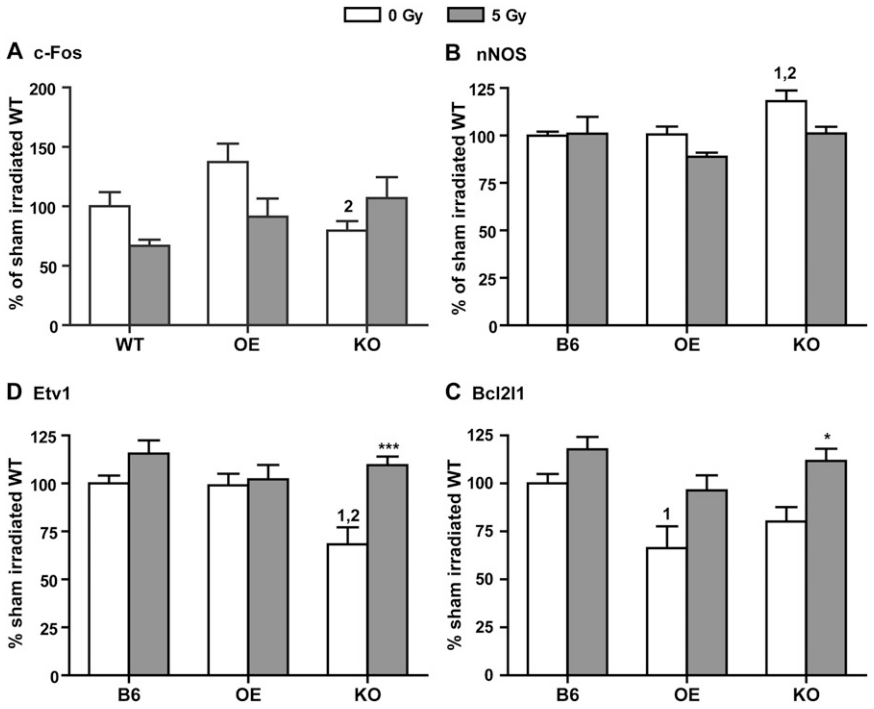

Fig. S6. Quantitative RT-PCR analyses of gene expression in the hippocampal formation. Expression levels of the immediate early gene c-Fos (*A*), neuronal-specific nitric oxide synthase (nNOS) (*B*), the transcription factor Etv1 (*C*), and the BCl2-like protein Bcl2l1 (*D*) were determined and compared between sham and irradiated WT, OE, and KO mice. All data (mean ± SEM) are compared with sham irradiated WT and expressed as percent sham-irradiated WT levels. Two-way ANOVA with Bonferroni posttest was carried out. $*P < 0.05$; $***P < 0.001$ for comparison between 0 and 5 Gy within each genotype. 1, $P < 0.05$ compared with sham irradiated WT; 2, $P < 0.05$ compared with sham irradiated OE mice.

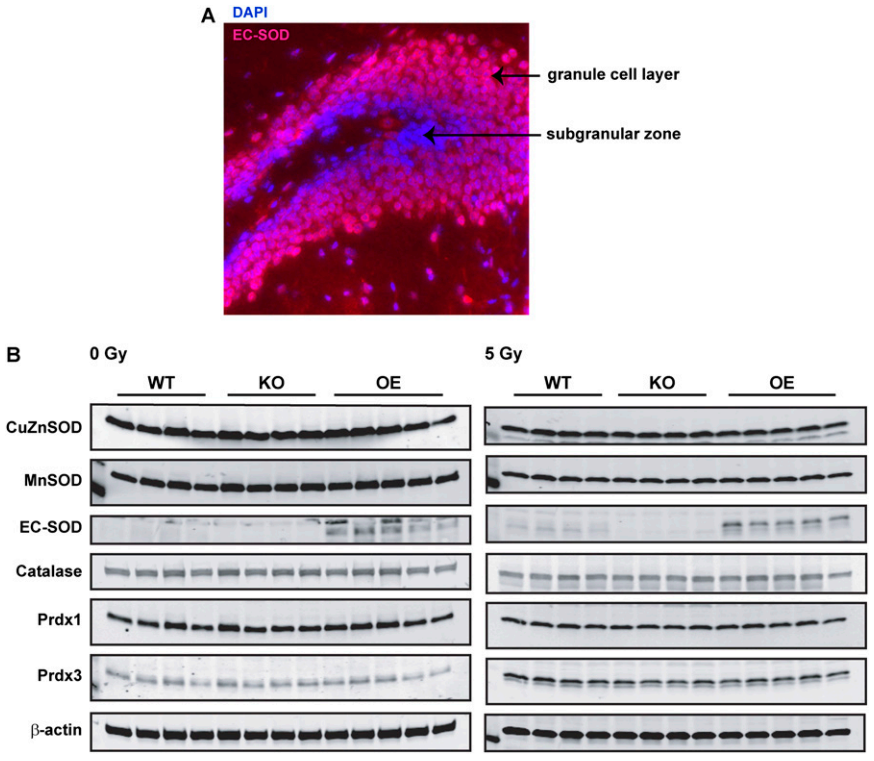

Fig. S7. Immuno-detection of EC-SOD and other antioxidant enzymes. (*A*) Immunohistochemical staining of EC-SOD in the dentate gyrus of OE mice. A representative picture showing EC-SOD stained in red with a rabbit polyclonal antibody and cell nuclei stained in blue with DAPI. A layer of blue cells in the SGZ indicates the EC-SOD–null status, and the red signals in granule cells indicate high levels of EC-SOD in this cell population. (*B*) Western blot analyses of tissue extracts from the hippocampal formation of sham and irradiated WT, OE, and KO mice. No overt changes in major antioxidant enzymes was observed in all experimental cohorts. Prdx1, peroxiredoxcin-1; Prdx3, peroxiredoxcin-3. β-actin was used as a loading control. $n = 4$, 4, and 5 for WT, KO, and OE, respectively.

Table S1. Summary of cell counts and percentage calculation

	WT		OE		KO	
Cells	0 Gy	5 Gy	0 Gy	5 Gy	0 Gy	5 Gy
$BrdU^+$ cells (short-term)	4,074 ± 131	2,538 ± 123	3,049 ± 372	2,310 ± 185	3,049 ± 128	2,657 ± 230
Dcx^+ cells	34,661 ± 1,191	20,568 ± 1448	22,894 ± 1,253	19,562 ± 1,593	17,350 ± 699	18,185 ± 1,992
Cat. E and F Dcx^+ cells	7,591 ± 626	7,331 ± 601	11,239 ± 476	10,114 ± 625	4,502 ± 584	6,790 ± 990
$BrdU^+$ cells (long-term)	2,560 ± 144	1,242 ± 42	1,870 ± 140	2,068 ± 111	734 ± 85	898 ± 101
Total $BrdU^+/NeuN^+$ cells	2,071 ± 124	721 ± 109	1,504 ± 130	1,790 ± 102	535 ± 92	548 ± 95
$BrdU^+/NeuN^+$ cells (as % $BrdU^+$)	80.9 ± 1.7%	67.7 ± 2.5%	87.2 ± 1.9%	83.3 ± 2.8%	81.3 ± 4.1%	61.5 ± 4.7%
Total $BrdU^+/GFAP^+$ cells	310 ± 33	251 ± 38	141 ± 27	229 ± 52	92 ± 22	230 ± 32
$BrdU^+/GFAP^+$ cells (as % $BrdU^+$)	12.2 ± 1.3%	23.7 ± 0.8%	8.0 ± 1.3%	10.4 ± 2.2%	14.9 ± 3.6%	30.0 ± 4.9%
Spine density (per 10 μm)	12.91 ± 0.55	9.81 ± 0.98	10.88 ± 0.48	12.67 ± 0.68	12.14 ± 0.73	11.43 ± 0.93
c-Fos^+ cells	643 ± 114	449 ± 106	1234 ± 129	942 ± 117	791 ± 201	338 ± 94
$BrdU^+/NeuN^+$ (as % Dcx^+ cells)	6.0%	3.5%	6.6%	9.2%	3.1%	3.0%

Table S2. Primers used for quantitative RT-PCR analyses

Gene	Forward primer	Reverse primer
Bcl2l1	5′-GGG ATG GAG TAA ACT GGG GTC-3′	5′-TGT TCC CGT AGA GAT CCA CAA A-3′
Bdnf	5′-TCA TAC TTC GGT TGC ATG AAG G-3′	5′-AGA CCT CTC GAA CCT GCC C-3′
Efna5	5′-ATT CCA GAG GGG TGA CTA CCA-3′	5′-GTG AGG GCA GAA AAC ATC CAG-3′
Etv1	5′-GCA AGT GCC TTA CGT GGT CA-3′	5′-CTT CAG CAA GCC ATG TTT CTT-3′
Fos	5′-CGG GTT TCA ACG CCG ACT A-3′	5′-TTG TCA CTA GAG ACG GAC AGA-3′
GAPDH	5′-TGG CAA AGT GGA GAT TGT TGC C-3′	5′-AAG ATG GTG ATG GGC TTC CCG-3′
nNOS	5′-CTG GTG AAG GAA CGG GTC AG-3′	5′-CCG ATC ATT GAC GGC GAG AAT-3′
Nr4a2	5′-GTG TTC AGG CGC AGT ATG G-3′	5′-TGG CAG TAA TTT CAG TGT TGG T-3′
Ntf3	5′-GGA GTT TGC CGG AAG ACT CTC-3′	5′-GGG TGC TCT GGT AAT TTT CCT TA-3′
Sema 3C	5′-CAA AAT GGC TGG CAA AGA TCC-3′	5′-TCC CCG GTT CAG GTA GGT G-3′